The following publication Y. Yang, "Development of Front-End Monitoring of Mutual Coupling and Load Conditions in Wireless Power Transfer Systems," 2020 8th International Conference on Power Electronics Systems and Applications (PESA), 2020, pp. 1-5 is available at https://doi.org/10.1109/PESA50370.2020.9344028

Development of Front-End Monitoring of Mutual Coupling and Load Conditions in Wireless Power Transfer Systems

Yun Yang[a]
[a]Department of Electrical Engineering, The Hong Kong Polytechnic University, Hong Kong, China
Email: yun1989.yang@polyu.edu.hk

Abstract–Recent advancements of series-series (SS)-compensated wireless power transfer (WPT) technology have enabled its wide-spread applications in battery charging of portable devices, electric vehicles (EV), and medical implants. A conventional SS-compensated WPT system consists of an inverter at the transmitter side to maximize the overall system efficiency typically by phase control or frequency control, and a DC-DC converter at the receiver side to regulate the charging current and voltage of the battery load. However, the efficiency and dynamic response of the conventional WPT system is limited by the DC-DC converter in point-of-load applications. The concept of maximum energy efficiency tracking (MEET) sparked off more related studies. Fast control strategies for MEET strategies are subsequently investigated, which normally require feedback signals from the receiver to the transmitter via a wireless communication system to calculate the coupling coefficient or load conditions. The additional wireless communication system increases the volume and cost of the system. To this end, front-end monitoring strategies are proposed for SS-compensated WPT systems without an extra wireless communication system. This paper covers main content of the tutorial that is presented in 8th International Conference on Power Electronics Systems and Applications (PESA), in which the development of front-end monitoring strategies from the Wireless Power Research Group of the University of Hong Kong are described.

***Keywords*-Front-end monitoring strategies, series-series (SS)-compensated wireless power transfer (WPT), coupling coefficient, load condition.**

I. INTRODUCTION

EARLY investigations of non-radiative WPT via near-field magnetically coupled resonators can be traced back to the late 19th century by Nicola Tesla [1]. Based on his inventions, non-radiative WPT are applied in transcutaneous systems, inductive power pick-up systems and portable electronics systems in the 1970s, 1990s and 2000s, respectively [2-4]. The dawn of mobile phones in the 1990s accelerates the development of non-radiative wireless power transfer (WPT) and triggers the foundation of Wireless Power Consortium (WPC) [5]. The eight founders of WPC made an agreement to adopt inductive coupling in the world first wireless standard "Qi". By far, more than 3700 "Qi-certified" products have been registered with WPC by over companies worldwide [6]. Although "Qi" is the earliest published specification for near-field WPT, it is not the only standard. The A4WP proposed by AirFuel Alliance (AFA) [7] and SAE TIR J2954 launched by Society of Automotive Engineers (SAE) [8] are the two alternative industrial guidelines that primarily focus on multiple charging devices and high-power applications in light-duty electric and plug-in electric vehicles, respectively. The key features of the three industrial guidelines are quite different. However, the three guidelines have a common feature that is the adoption of Tesla's principle to compensate the leakage inductance in the power flow path to ensure high transmission efficiency by various compensation topologies, such as series-series (SS), series-parallel (SP), parallel-parallel (PP), parallel-series (PS), LCL-S, LCL-P, LCL-LCL, LCL-LCC, LCC-S, LCC-P, LCC-LCC, LCC-LCL, and other hybrid compensations [9]. Among them, the SS-compensation is most widely adopted due to its design being independent of load and coupling coefficient [10].

In practical SS-compensated WPT systems, communication devices are often adopted to ensure reliable and high-efficiency operations by delivering feedback signals from the user-ends to the front-ends. However, the communication devices quite annoy manufactures by enhancing complexity, bringing additional costs, and deteriorating dynamic performance of WPT systems [11-13]. More importantly, an exclusive communication standard may be adopted, which is undesirable by most manufactures. To reduce this anxiety, front-end monitoring strategies are developed by the research groups worldwide [14-23]. Apart from the eliminations of communication devices, the front-end monitoring strategies for the parameters, such as mutual inductances and load resistances, can also improve the dynamic performance and overall transfer efficiency when the operation conditions vary [24, 25]. Besides, some front-end monitoring strategies can also detect the ageing effect of receiving coils and loads by monitoring their equivalent impedances [22].

This paper focus on various front-end monitoring strategies that has been developed by the Wireless Power Research Group of the University of Hong Kong so far. The roadmap of the front-end monitoring strategies is presented in the tutorial session "Development of Front-end Monitoring of Mutual Coupling and Load Conditions in Wireless Power Transfer Systems" of the 8th International Conference on Power Electronics Systems and Applications (PESA). The early monitoring method is designed based on the measurements of the input voltage and current to solely estimate the load impedance of an SS-compensated WPT system [18]. However, only one load impedance can be estimated by this monitoring method and mutual inductances are required to be preliminarily known. To this end, an advanced monitoring method is presented for monitoring two loads in a four-coil SS-compensated WPT system using only the input voltage and input current measurements [19]. Besides, research is extended to show that not only the load resistance but also the mutual inductance can be estimated simultaneously with the input voltage and input current measurements at one operating frequency by modifying the monitoring equations [20]. Simplified estimation equations, which can be easily implemented using inexpensive digital controllers, are further developed in [21]. Nevertheless, the parameter deviations will affect the accuracies of the monitoring strategies in [20] and [21]. To address this critical issue, a two-layer adaptive Differential Evolution (ADE) algorithm is proposed to monitor not only the mutual inductances and

load resistances, but also the parameters of the receivers of SS-compensated WPT systems [22]. These "model-based" monitoring methods for determining the mutual coupling coefficient require mathematical calculations based on fundamental equivalent circuits of WPT systems and the performance highly depends on the computation speed of the processors. Alternatively, a very fast "hardware-based" monitoring strategy is proposed to accurately and rapidly monitor the mutual coupling coefficients of SS-compensated WPT systems [23]. This paper reviews both the "model-based" and "hardware-based" monitoring methods for SS-compensated WPT systems in [18-23]. Conclusions and future works are also discussed.

II. "Model-Based" Monitoring Strategies

A. *Single Load Monitoring*

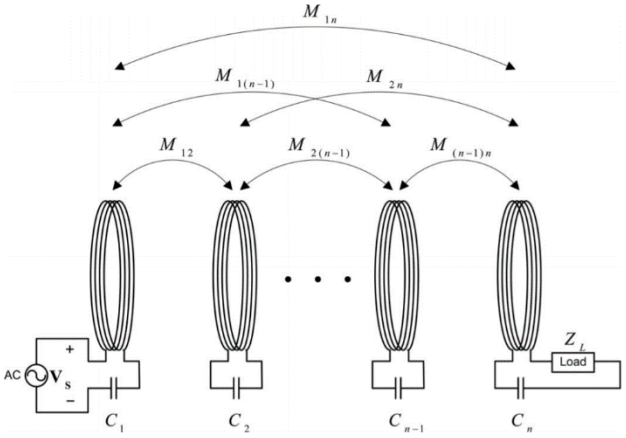

Fig. 1. Schematic of an *n*-coil wireless power transfer system with one load [18].

For an *n*-coil SS-compensated WPT system with only one load, as shown in Fig. 1, based on the Kirchhoff's voltage law, the system can be described in a general matrix as

$$\begin{bmatrix} V_s \\ 0 \\ \vdots \\ 0 \\ 0 \end{bmatrix} = \begin{bmatrix} Z_1 & j\omega M_{12} & \cdots & j\omega M_{1(n-1)} & j\omega M_{1n} \\ j\omega M_{12} & Z_2 & \cdots & j\omega M_{2(n-1)} & j\omega M_{2n} \\ \vdots & \vdots & \ddots & \vdots & \vdots \\ j\omega M_{1(n-1)} & j\omega M_{2(n-1)} & \cdots & Z_{n-1} & j\omega M_{(n-1)n} \\ j\omega M_{1n} & j\omega M_{2n} & \cdots & j\omega M_{(n-1)n} & Z_n + Z_L \end{bmatrix} \times \begin{bmatrix} \mathbf{I_1} \\ \mathbf{I_2} \\ \vdots \\ \mathbf{I_{n-1}} \\ \mathbf{I_n} \end{bmatrix} \quad (1)$$

where V_s is the input AC input voltage of the transmitter. Z_1, Z_2, …, Z_{n-1}, Z_n are the equivalent impedances of the transmitter and receiver resonators. Z_L is the load impedance. M_{ij} indicates the mutual inductance between the *i*-th coil and the *j*-th coil (i.e., M_{ij}=M_{ji}). In the system model (1), the coils are coupled to each other while the load is not coupled to any one of the coils. Therefore, the load, including both the resistance and reactance, is independent of the coils in the system. The load can be either linear or nonlinear load.

By applying Cramer's rule, the load impedance Z_L can be derived based on the system model as

$$Z_L = \frac{D_n}{D_{n-1}} \quad (2)$$

where $D_{n-1} = \begin{vmatrix} j\omega M_{12} & j\omega M_{13} & \cdots & \mathbf{V_s} - Z_1\mathbf{I_1} & 0 \\ Z_2 & j\omega M_{23} & \cdots & -j\omega M_{12}\mathbf{I_1} & 0 \\ \vdots & \vdots & \ddots & \vdots & \vdots \\ j\omega M_{2(n-1)} & j\omega M_{3(n-1)} & \cdots & -j\omega M_{1(n-1)n}\mathbf{I_1} & 0 \\ j\omega M_{2n} & j\omega M_{3n} & \cdots & -j\omega M_{1n}\mathbf{I_1} & 1 \end{vmatrix}$

and $D_n = \begin{vmatrix} j\omega M_{12} & j\omega M_{13} & \cdots & j\omega M_{1n} & \mathbf{V_s} - Z_1\mathbf{I_1} \\ Z_2 & j\omega M_{23} & \cdots & j\omega M_{2n} & -j\omega M_{12}\mathbf{I_1} \\ \vdots & \vdots & \ddots & \vdots & \vdots \\ j\omega M_{2(n-1)} & j\omega M_{3(n-1)} & \cdots & j\omega M_{(n-1)n} & -j\omega M_{1(n-1)n}\mathbf{I_1} \\ j\omega M_{2n} & j\omega M_{3n} & \cdots & Z_n & -j\omega M_{1n}\mathbf{I_1} \end{vmatrix}$.

The schematic diagram of the hardware setup and the experimental results in [18] are shown in Figs. 2 and 3, respectively. The load resistances are accurately monitored.

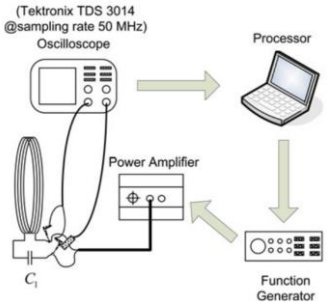

Fig. 2. Schematic diagram of the hardware setup in [18].

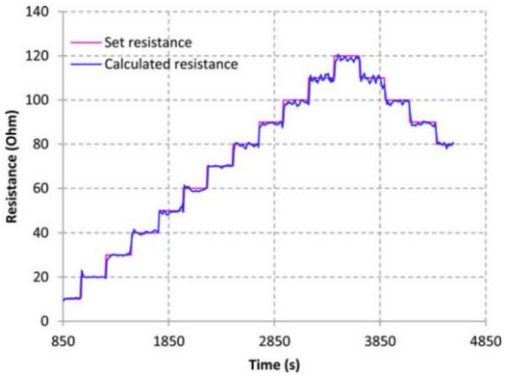

Fig. 3. Practical set resistance and the monitored resistance in [18].

B. *Two Loads Monitoring*

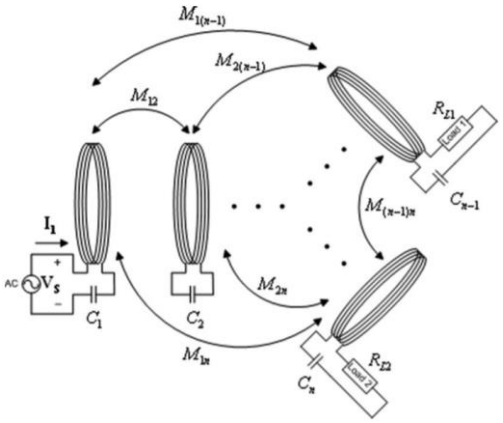

Fig. 4. Schematic of an *n*-coil wireless power transfer system with two loads [19].

For an *n*-coil SS-compensated WPT system with two loads, as shown in Fig. 4, based on the Kirchhoff's voltage law, the system can be described in a general matrix as

$$\begin{bmatrix} V_s \\ 0 \\ \vdots \\ 0 \\ 0 \end{bmatrix} = \begin{bmatrix} Z_1 & j\omega M_{12} & \cdots & j\omega M_{1(n-1)} & j\omega M_{1n} \\ j\omega M_{12} & Z_2 & \cdots & j\omega M_{2(n-1)} & j\omega M_{2n} \\ \vdots & \vdots & \ddots & \vdots & \vdots \\ j\omega M_{1(n-1)} & j\omega M_{2(n-1)} & \cdots & Z_{n-1} + R_{L1} & j\omega M_{(n-1)n} \\ j\omega M_{1n} & j\omega M_{2n} & \cdots & j\omega M_{(n-1)n} & Z_n + R_{L2} \end{bmatrix} \times \begin{bmatrix} \mathbf{I_1} \\ \mathbf{I_2} \\ \vdots \\ \mathbf{I_{n-1}} \\ \mathbf{I_n} \end{bmatrix} \quad (3)$$

where the two loads are purely resistive. By assuming R_{L1} is a known parameter, the system model in (3) can be rewritten as

$$\begin{bmatrix} \mathbf{I_2} \\ \mathbf{I_3} \\ \vdots \\ \mathbf{I_n} \\ R_{L2}\mathbf{I_n} \end{bmatrix} = \mathbf{P} \times \begin{bmatrix} \mathbf{V_s} - Z_1\mathbf{I_1} \\ -j\omega M_{12}\mathbf{I_1} \\ \vdots \\ -j\omega M_{1(n-1)n}\mathbf{I_1} - R_{L1}\mathbf{I_{n-1}} \\ -j\omega M_{1n}\mathbf{I_1} \end{bmatrix} \quad (4)$$

where $\mathbf{P} = \begin{bmatrix} j\omega M_{12} & j\omega M_{13} & \cdots & j\omega M_{1n} & 0 \\ Z_2 & j\omega M_{23} & \cdots & j\omega M_{2n} & 0 \\ \vdots & \vdots & \ddots & \vdots & \vdots \\ j\omega M_{2(n-1)} & j\omega M_{3(n-1)} & \cdots & j\omega M_{(n-1)n} & 0 \\ j\omega M_{2n} & j\omega M_{3n} & \cdots & Z_n & 1 \end{bmatrix}^{-1}$.

The last three equations in (4) are

$$\mathbf{I_{n-1}} = a + bR_{L1}\mathbf{I_{n-1}} \quad (5.1)$$

$$\mathbf{I_n} = c + dR_{L1}\mathbf{I_{n-1}} \quad (5.2)$$

$$R_{L2}\mathbf{I_n} = e + fR_{L1}\mathbf{I_{n-1}} \quad (5.3)$$

where

$$\begin{cases} a = \mathbf{P_{n-2}V} \\ b = -p_{(n-2)(n-1)} \\ c = \mathbf{P_{n-1}V} \\ d = -p_{(n-1)(n-1)} \\ e = \mathbf{P_nV} \\ f = -p_{n(n-1)} \end{cases}$$

$$\mathbf{V} = \begin{bmatrix} \mathbf{V_S} - Z_1\mathbf{I_1} \\ -j\omega M_{12}\mathbf{I_1} \\ \vdots \\ -j\omega M_{1(n-1)}\mathbf{I_1} \\ -j\omega M_{1n}\mathbf{I_1} \end{bmatrix}$$

$\mathbf{P}_i$ is the i-th row vector in matrix $\mathbf{P}$ and p_{ij} is the element of the i-th row and j-th column in the $\mathbf{P}$ matrix.

Based on (5.1)~(5.3), the relationships between the R_{L1} and R_{L2} can be derived as

$$AR_{L1}R_{L2} + BR_{L1} + CR_{L2} + D = 0 \quad (6)$$

where the four coefficients A, B, C and D are complex numbers, i.e.,

$$\begin{cases} A = ad - bc = \alpha_A + j\beta_A \\ B = be - af = \alpha_B + j\beta_B \\ C = c = \alpha_C + j\beta_C \\ D = -e = \alpha_D + j\beta_D \end{cases}$$

By reorganizing the real and imaginary terms and eliminating the nonlinear term $R_{L1}R_{L2}$, the equation (6) can be further derived as

$$(\alpha_B\beta_A - \alpha_A\beta_B)R_{L1} + (\alpha_C\beta_A - \alpha_A\beta_C)R_{L2} = \alpha_A\beta_D - \alpha_D\beta_A \quad (7)$$

Apparently, only two sets of **Vs** and $\mathbf{I_1}$ measurements at two different frequencies can be used to calculate the two load resistances in theory. Simulation results in Fig. 5 show that one intersection point of R_{L1} and R_{L2} can be plotted at various operating frequencies under ideal conditions.

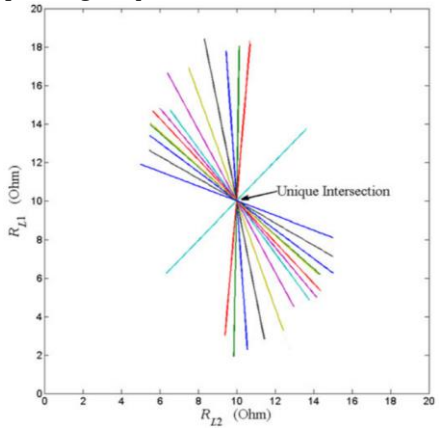

Fig. 5. One intersection points of the two loads at various operating frequencies under ideal conditions [19].

Experiments are conducted on a four-coil SS-compensated WPT system with two loads, as shown in Fig. 6. Based on 20 different frequency sweeping (20 equations are adopted), the two load resistances are monitored with high accuracy, as shown in Fig. 7.

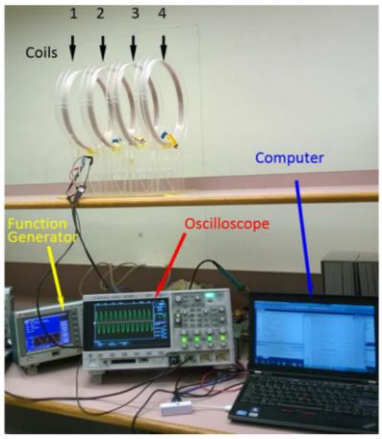

Fig. 6. Experimental setup in [19].

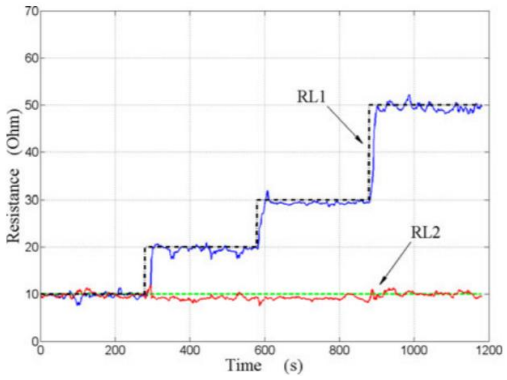

Fig. 7. Experimental results in [19].

C. Mutual Inductance and Single Load Monitoring

Based on the equivalent circuit of a two-stage SS-compensated WPT system, the system model in the frequency domain can be derived as

$$\begin{bmatrix} \mathbf{V_s} \\ 0 \end{bmatrix} = \begin{bmatrix} Z_1 & j\omega M_{12} \\ j\omega M_{12} & Z_2 + R_L \end{bmatrix} \begin{bmatrix} \mathbf{I_1} \\ \mathbf{I_2} \end{bmatrix} \quad (8)$$

where

$$Z_1 = R_1 + j\left(\omega L_1 - \frac{1}{\omega C_1}\right)$$

$$Z_2 = R_2 + j\left(\omega L_2 - \frac{1}{\omega C_2}\right)$$

ω is the switching angular frequency. Based on (8), the load resistance can be expressed as

$$R_L = \frac{R_L\mathbf{I_2}}{\mathbf{I_2}} = \frac{(\omega M_{12})^2 + Z_1Z_2 - Z_2Z_{\text{in}}}{Z_{\text{in}} - Z_1} = \frac{(\omega M_{12})^2}{Z_{\text{in}} - Z_1} - Z_2 \quad (9)$$

where $Z_{\text{in}} = \frac{V_S}{I_1}\angle\varphi$ is the input impedance which can be expressed in the vector form. For purely resistive loads, the imaginary part is zero. Then, the monitored mutual inductance and load resistance can be derived as

$$M_{12} = \sqrt{\frac{\omega L_2 - \frac{1}{\omega C_2}}{\omega^2 \mathbf{Im}(Z_{\text{in}} - Z_1)^{-1}}} \quad (10)$$

$$R_L = \frac{\omega L_2 - \frac{1}{\omega C_2}}{(Z_{\text{in}} - Z_1)\mathbf{Im}(Z_{\text{in}} - Z_1)^{-1}} - Z_2 \quad (11)$$

Experiments are conducted on the coils with different positions in [20]. The load resistance is 25.8 Ω while the

mutual inductances are changed from (a) the initial position about 23 μH to (b) the axial separation about 16 μH to (c) the lateral misalignment about 21 μH to (d) the angular misalignment about 16.7 μH. Obviously, the proposed monitoring strategy can accurately monitor the load resistance and the mutual inductances simultaneously.

(a) (b) (c) (d)

Fig. 8. Different coil positions in [20].

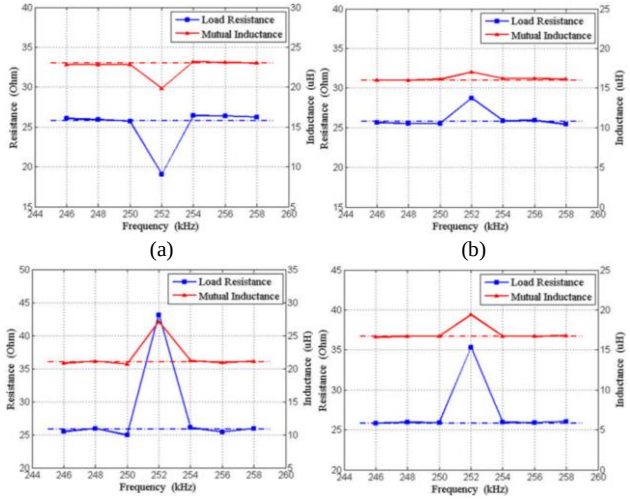

(a) (b) (c) (d)

Fig. 9. Monitoring results for the load resistance and mutual inductances in [20].

The load monitoring equation is further simplified in [21], which can be implemented using inexpensive digital controllers. Besides, the monitoring errors caused by the parameter drifts and measurement errors are mitigated as compared to the conventional monitoring strategy. The load monitoring equation in [21] is

$$R_L = \frac{Z_s V_{in} \cos\theta - R_p Z_s I_p}{V_{in} \sin\theta + Z_p I_p} - R_s \quad (a \neq 1) \qquad (12)$$

where $Z_p = \left(\frac{a^2-1}{a}\right)\omega_o L_p$ and $Z_s = \left(\frac{a^2-1}{a}\right)\omega_o L_s$. ω_o is nominal angular frequency of the input voltage. a is the frequency ratio. θ is the phase angle between the input voltage and the transmitter current. I_p is the amplitude of the transmitter current. The schematic diagram of the load monitoring strategy in [21] is shown in Fig. 10.

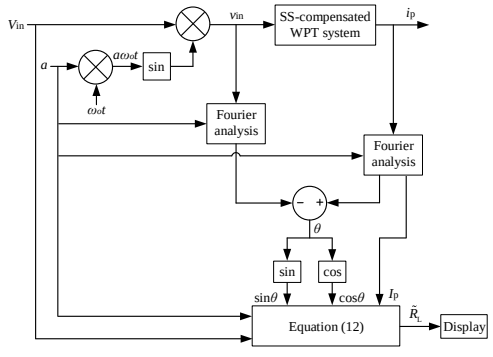

Fig. 10. Schematic diagram of the load monitoring strategy in [21].

The simulation results of the two-stage SS-compensated WPT system in [21] with the input voltage of 61.12 V, load resistances of 10 Ω and 50 Ω, and different mutual inductances are shown in Fig. 11.

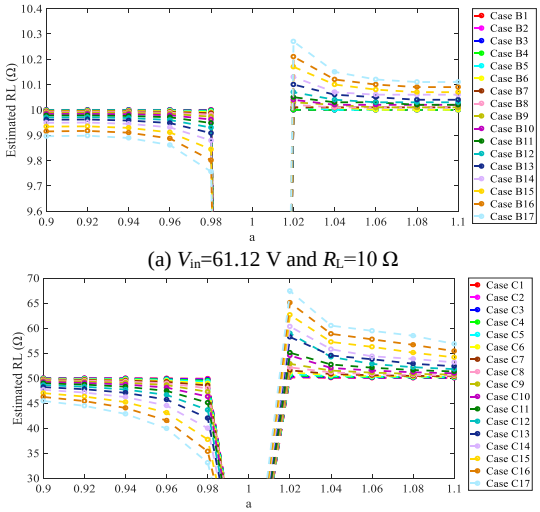

(a) V_{in}=61.12 V and R_L=10 Ω

(b) V_{in}=61.12 V and R_L=50 Ω

Fig. 11. Simulation results in [21].

D. Heuristic Algorithm Method

The pioneers have developed several different monitoring strategies to effectively monitor one or two loads and mutual inductances of SS-compensated WPT systems [18-21]. However, these methods are invalidated for WPT systems with multiple loads and unknown parameters of the receivers. To bridge the research gaps, heuristic algorithms are adopted in [22] to monitor the mutual inductances, load resistances and the parameters of the receivers, simultaneously.

A typical SS-compensated WPT system with multiple outputs is shown in Fig. 12 and the its equivalent circuit at the fundamental frequency is plotted in Fig. 13. The DC voltage (i.e., V_{dc}) is converted to a high-frequency alternating voltage v_p by a phase shift control being applied to a full-bridge inverter with the duty ratio of 0.5. The parameters of the transmitter comprise the coil inductance L_p, compensated capacitance C_p, and the equivalent-series-resistance (ESR) R_p. The receiver resonators comprise the coil inductances L_{si} (i=1, 2, …, m), compensated capacitances C_{si} (i=1, 2, …, m), the ESR R_{si} (i=1, 2,…, m), and the load resistances R_{Li} (i=1, 2,…, m). M_i (i=1, 2,…, m) are the mutual inductances between the transmitting coil and the receiving coils. M_{ij} (i=1, 2,…, m, j=1, 2,…, m, $i \neq j$) are the mutual inductances between the receiving coils. v_{p1}, v_{o1i}, i_{p1}, and i_{s1i} are fundamental components. R_{eq1i} (i=1, 2,…, m) are the equivalent resistances of the receiving resonators, R_{eq1i}. Besides, the "self-mutual inductances" are physically null (i.e. M_{11}=M_{22}=…=M_{mm}=0).

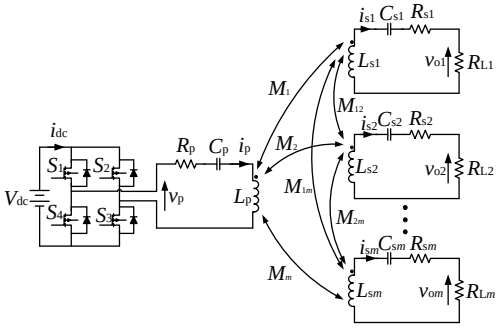

Fig. 12. Topology of an SS-compensated WPT system with multiple outputs.

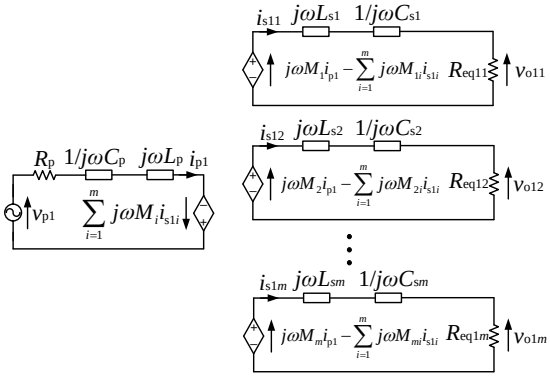

Fig. 13. Equivalent circuit of an SS-compensated WPT system at the fundamental frequency with multiple outputs.

Based on the equivalent circuit in Fig. 13,

$$\begin{cases} v_{p1} = \left[R_p + \left(\omega L_p - \frac{1}{\omega C_p}\right)j\right] i_{p1} - \omega \mathbf{M}^T \mathbf{i_{s1}} j \\ \omega \mathbf{M} i_{p1} j - \omega \mathbf{M_1} \mathbf{i_{s1}} j = \mathbf{Z_s} \mathbf{i_{s1}} \end{cases}, \quad (13)$$

where $\mathbf{i_{s1}} = [i_{s11}, i_{s12}, \cdots i_{s1m}]^T$, $\mathbf{M} = [M_1, M_2, \cdots M_m]^T$, $\mathbf{M_1} = \begin{bmatrix} 0 & M_{12} & \cdots & M_{1m} \\ M_{21} & 0 & \cdots & M_{2m} \\ \vdots & \vdots & \ddots & \vdots \\ M_{m1} & M_{m2} & \cdots & 0 \end{bmatrix}$, $\mathbf{Z_s} = \begin{bmatrix} Z_{s1} & 0 & \cdots & 0 \\ 0 & Z_{s2} & \cdots & 0 \\ \vdots & \vdots & \ddots & \vdots \\ 0 & 0 & \cdots & Z_{sm} \end{bmatrix}$, and $Z_{si} = R_{eq1i} + \left(\omega L_{si} - \frac{1}{\omega C_{si}}\right)j \ (i = 1,2,\cdots m)$.

To simplify (13) by cancelling the term $\mathbf{i_{s1}}$,

$$\frac{v_{p1}}{i_{p1}} = Z_{p1} = R_p + \left(\omega L_p - \frac{1}{\omega C_p}\right)j + \omega^2 \mathbf{M}^T (\omega \mathbf{M_1} j + \mathbf{Z_s})^{-1} \mathbf{M} \quad (14)$$

where Z_{p1} is the equivalent impedance of the SS-compensated WPT system at the fundamental frequency. By separating the real and imaginary parts in (14),

$$\frac{v_{p1}}{i_{p1}} = \mathbf{Re}(Z_{p1}) + \mathbf{Im}(Z_{p1}) = \left(R_p + \omega^2 P(\mathbf{M}, \mathbf{M_1}, \mathbf{Z_s}, \omega)\right) + \left(\omega L_p - \frac{1}{\omega C_p} + \omega^2 Q(\mathbf{M}, \mathbf{M_1}, \mathbf{Z_s}, \omega)\right)j \quad (15)$$

where the real and imaginary parts of Z_{p1} are

$$\mathbf{Re}(Z_{p1}) = R_p + \omega^2 P(\mathbf{M}, \mathbf{M_1}, \mathbf{Z_s}, \omega) \quad (16)$$

$$\mathbf{Im}(Z_{p1}) = \left(\omega L_p - \frac{1}{\omega C_p} + \omega^2 Q(\mathbf{M}, \mathbf{M_1}, \mathbf{Z_s}, \omega)\right)j \quad (17)$$

The scalars $P(\mathbf{M}, \mathbf{M_1}, \mathbf{Z_s}, \omega)$ and $Q(\mathbf{M}, \mathbf{M_1}, \mathbf{Z_s}, \omega)$ are determined by the values of $\mathbf{M}$, $\mathbf{M_1}$, $\mathbf{Z_s}$ and ω. By sweeping the switching angular frequency ω from the lower bound ω_L to the upper bound ω_H, the equivalent impedance Z_{p1} of the SS-compensated WPT system at the fundamental frequency can vary. Apparently, the equivalent impedance Z_{p1} is determined by the parameters L_p, C_p, R_p, L_{si}, C_{si}, R_{eq1i}, $\mathbf{M}$, and $\mathbf{M_1}$,

$$\begin{cases} \frac{v_{p1l}}{i_{p1l}} = Z_{p1l} = f(L_p, C_p, R_p, L_{si}, C_{si}, R_{eq1i}, \mathbf{M}, \mathbf{M_1}, \omega_l) \\ \omega_L \le \omega_l \le \omega_H \end{cases} \quad (18)$$

In practice, the parameters of the transmitter, i.e., L_p, C_p and R_p, are preliminarily known. Then, the identification model for the parameters of the receivers and the mutual inductances can be derived as

$$\min J = \left\| \mathbf{v_{p1est}} - \mathbf{v_{p1}} \right\| \quad (19)$$

s.t. $\mathbf{v_{p1est}} = \mathbf{i_{p1}} \mathbf{Z_{p1}}$, $\omega_L \le \omega_l \le \omega_H$, $L_{siL} \le L_{si} \le L_{siH}$, $C_{siL} \le C_{si} \le C_{siH}$, $R_{eq1iL} \le R_{eq1i} \le R_{eq1iH}$, $\mathbf{M_L} \le \mathbf{M} \le \mathbf{M_H}$, and $\mathbf{M_{1L}} \le \mathbf{M_1} \le \mathbf{M_{1H}}$ $(i = 1,2,\cdots m)$ $(j = 1,2,\cdots n)$,

where $\mathbf{Z_{p1}} = \begin{bmatrix} Z_{p11} & 0 & \cdots & 0 \\ 0 & Z_{p12} & \cdots & 0 \\ \vdots & \vdots & \ddots & \vdots \\ 0 & 0 & \cdots & Z_{p1m} \end{bmatrix}$. The objective of the identification model is to minimize the voltage differences between the estimated input voltages $\mathbf{v_{p1est}}$ and the measured input voltages $\mathbf{v_{p1}}$. The estimated voltages $\mathbf{v_{p1est}}=[v_{p1est1}, v_{p1est2},\ldots, v_{p1estn}]$ are calculated by the equation $\mathbf{v_{p1est}}=\mathbf{i_{p1}}\mathbf{Z_{p1}}$ based on the measured transmitting currents $\mathbf{i_{p1}}=[i_{p11}, i_{p12},\ldots, i_{p1n}]$ and the searching parameters of L_{si}, C_{si}, R_{eq1i}, $\mathbf{M}$, and $\mathbf{M_1}$ at the switching angular frequencies ω_l $(l=1, 2,\ldots, n)$. The identified parameters L_{si}, C_{si}, R_{eq1i}, $\mathbf{M}$, and $\mathbf{M_1}$ are searched within the lower bounds of L_{si}L, C_{si}L, R_{eq1i}L, $\mathbf{M_L}$, $\mathbf{M_{1L}}$ and the upper bounds of L_{si}H, C_{si}H, R_{eq1i}H, $\mathbf{M_H}$, $\mathbf{M_{1H}}$. The values of the bounds are determined empirically.

Different heuristic algorithms can be applied to optimize the objective function in (19). In [22], two conventional heuristic algorithms, i.e., Genetic Algorithm (GA) and Adaptive Differential Evolution (ADE), and one new heuristic algorithm, i.e., two-layer ADE, are adopted to monitor the mutual inductances, load resistances and unknown parameters of the receivers, simultaneously. Details of the algorithms can be found in [22]. Experiments are conducted on two-coil and three-coil SS-compensated WPT systems, as shown in Fig. 14.

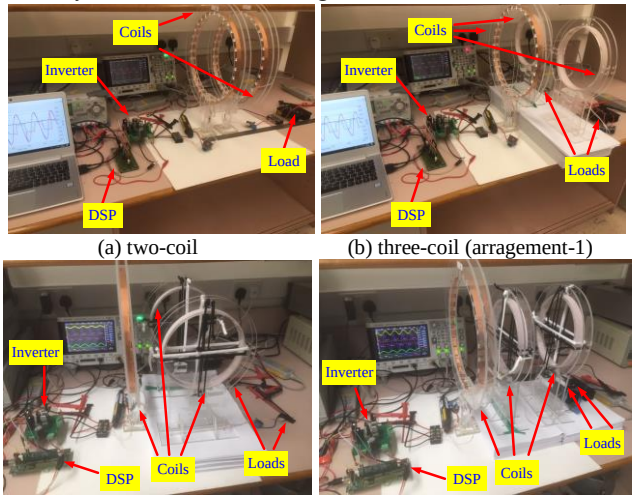

(a) two-coil (b) three-coil (arragement-1)
(c) three-coil (arragement-2) (d) three-coil (arragement-3)

Fig. 14. Experimental setups in [22].

For the two-coil SS-compensated WPT system, the comparisons of the average relative errors and standard deviations between the GA and the ADE are shown in Fig. 15. Apparently, the average relative errors of the monitored parameters can be reduced about 1% for L_s, 0.8% for C_s, 10.4% for R_{eq1}, and 4.6% for M. The standard deviations of the monitored parameters in all the cases are also significantly reduced. The results also demonstrate that the ADE can monitor the parameters of two-coil SS-compensated WPT systems more steadily and accurately than the GA. The comparisons of the average relative errors and standard deviations between the ADE and the two-layer ADE are shown in Fig. 16. The results show that the monitoring performances of the two-layer ADE are almost the same as the ADE for the two-coil SS-compensated WPT systems.

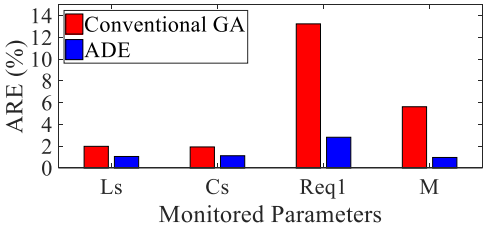

(a) average relative errors

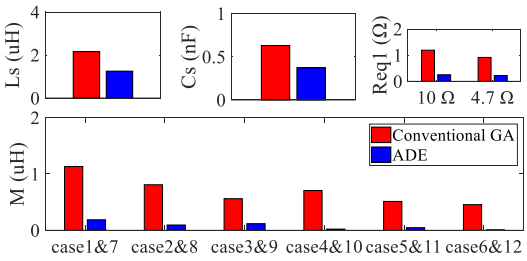

(b) standard deviations

Fig. 15. Comparisons between GA and ADE for the two-coil WPT system in different cases [22].

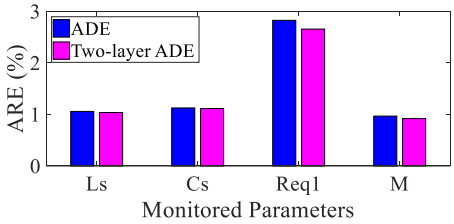

(a) average relative errors

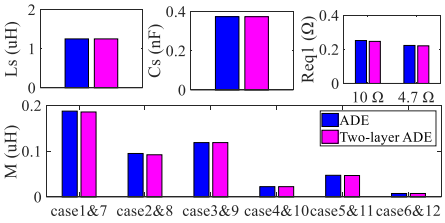

(b) standard deviations

Fig. 16. Comparisons between ADE and two-layer ADE for the two-coil WPT system in different cases [22].

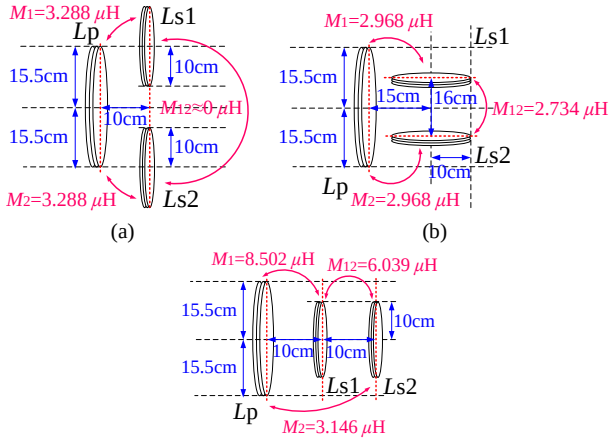

Fig. 17. (a) Arragenment-1, (b) Arrangement-2 and (c) Arragement-3 of the three-coil WPT system [22].

However, for the three-coil SS-compensated WPT system (details of the three arrangements are shown in Fig. 17), the performance of the two-layer ADE and the ADE are different. The comparisons of the average relative errors and standard deviations among the three algorithms are shown in Fig. 18. Obviously, in all the three arrangements, the performances of the average relative errors and the standard deviations of the two-layer ADE are the best. The ADE is better than the conventional GA. Nevertheless, the computation time of the two-layer ADE is longer than that of the ADE, while the computation time of the ADE is longer than that of the conventional GA.

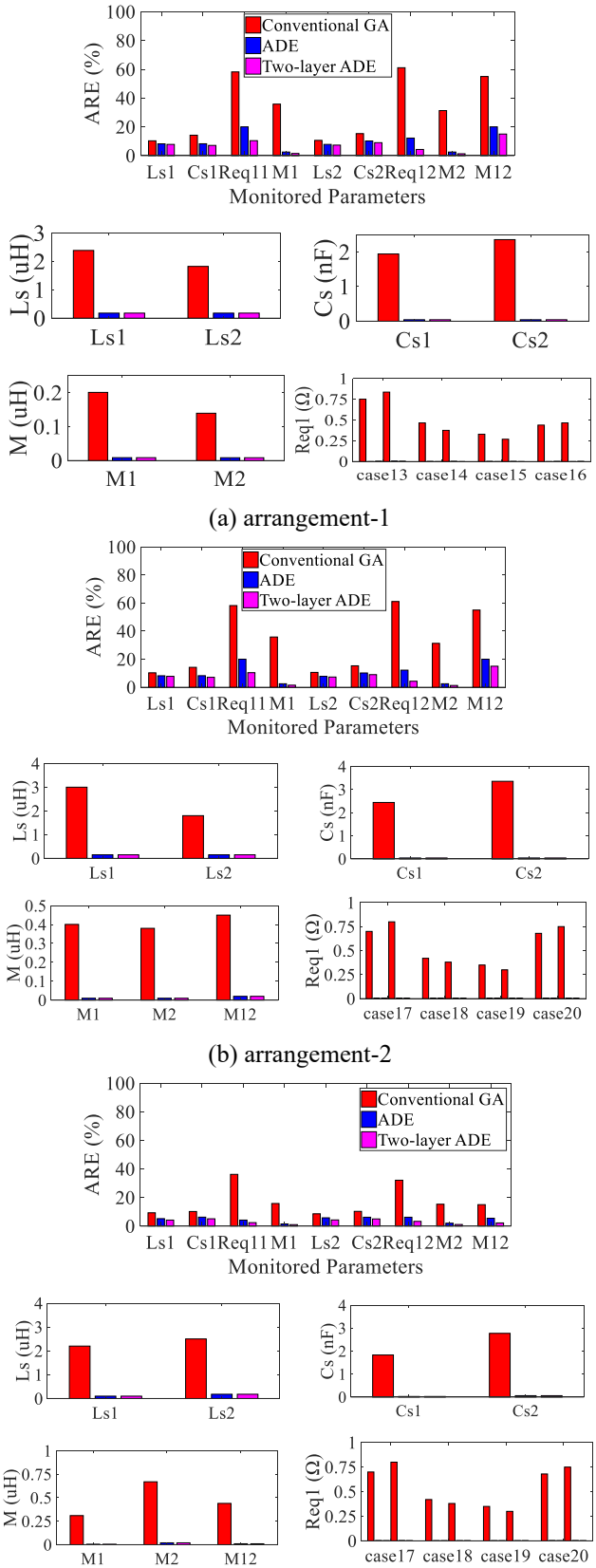

Fig. 18. Comparisons among GA, ADE and two-layer ADE for the three-coil WPT system in different cases [22].

III. "Hardware-Based" Monitoring Strategy

For the "model-based" methods, the parameter values of the transmitter and receiver resonators need to be preliminarily known. For some SS-compensated WPT systems, the sensitivities of the parasitic parameters are

high. Besides, for those heuristic algorithm methods, the total monitoring time is quite long and the algorithms are too complicated to be implemented using inexpensive digital controllers. To this end, a "hardware-based" monitoring method is proposed in [23]. However, the "hardware-based" monitoring method is only validated for SS-compensated WPT systems with active rectifiers (some commonly used active rectifiers as shown in Fig. 19).

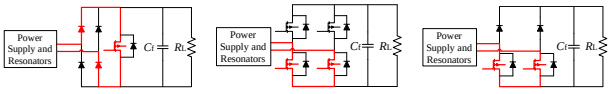

(a) (b) (c)

Fig. 19. Some examples of active rectifiers in SS-compensated WPT systems.

The "hardware-based" monitoring strategy is carried out by short-circuiting the outputs of active rectifiers. Therefore, the proposed monitoring strategy can be adopted for the SS-compensated WPT systems with various types of loads. Compared to the "model-based" monitoring strategies by measuring both the fundamental components of the input voltage and the transmitter current, the proposed "hardware-based" monitoring strategy only measures the phase difference between the switching signal of the inverter and the transmitter current. Besides, the "hardware-based" method can simultaneously achieve fast monitoring of the coupling coefficient using inexpensive digital controllers and high accuracy even for the systems with unknown parameters of the resonators, while the existing "model-based" methods cannot. The block diagram of digital controller for determination of coupling coefficient is shown in Fig. 20. Details of the "hardware-based" method can be found in [23].

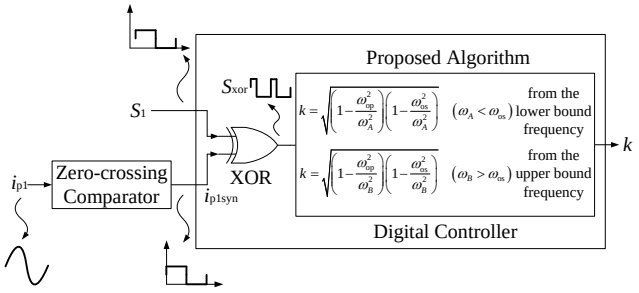

Fig. 20. The block diagram of a digital controller for determination of coupling coefficient [23].

In order to determine ω_A, the power inverter's frequency is scanned from the lower bound frequency $f_{\min}$. Fig. 21 shows the flow chart of determining ω_A and then k. The duty cycle of the signal S_{XOR} is detected and represented as a digitized signal $D_p(N)$. If this duty cycle is smaller than the previous duty cycle (i.e., $D_p(N)<D_p(N\text{-}1)$), the switching frequency will increase. This process will continue until $D_p(N)$ approaches zero when ω_A is reached. Then, the coupling coefficient can be determined. The timing diagram of typical waveforms are shown in Fig. 22. Similar flow chart of determining ω_B and then k, and the corresponding timing diagram of typical waveforms can be found in [23]. Experiments are carried out on an SS-compensated WPT system with a semi-bridgeless rectifier, as shown in Fig. 23. The adopted resonators are shown in Fig. 24. The specifications of the resonators are provided in Table I.

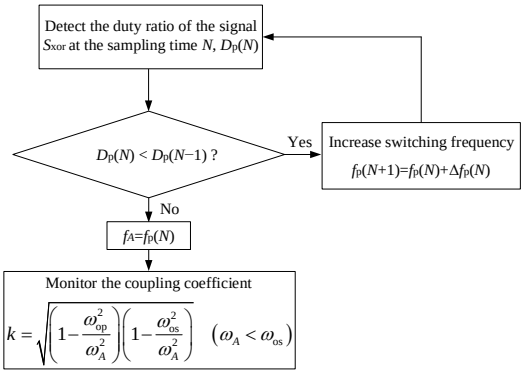

Fig. 21. The flow chart of the monitoring strategy to determine ω_A and then k [23].

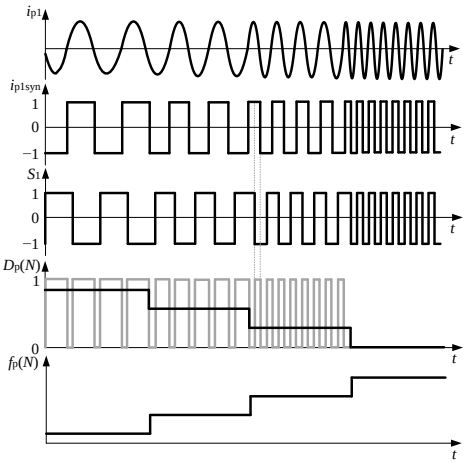

Fig. 22. Timing diagrams of the monitoring strategy to determine ω_A and then k [23].

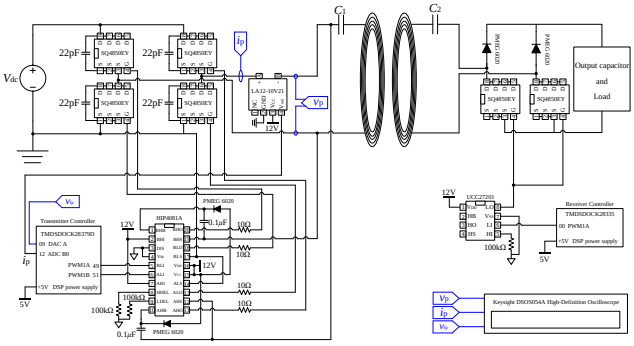

Fig. 23. Full hardware schematic diagram of the WPT system in experiment [23].

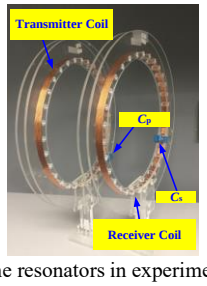

Fig. 24. Photograph of the resonators in experiment [23].

TABLE I. SPECIFICATIONS OF THE RESONATORS [23]

Parameter	Value
Coil diameter of both transmitter and receiver coils	31 cm
Wire diameter of both transmitter and receiver coils	1.2 mm
Number of turns of transmitter and receiver coils	11
Length of the winding of transmitter and receiver coils	15 mm
L_p @ 100 kHz	91.78 μH
C_p @ 100 kHz	27.2 nF
R_p @ 100 kHz	0.95 Ω
L_s @ 100 kHz	92.05 μH
C_s @ 100 kHz	26.9 nF
R_s @ 100 kHz	1.06 Ω

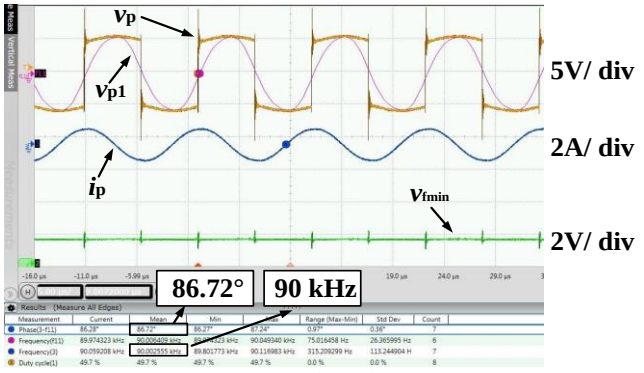

(a) at 90 kHz (f_{min})

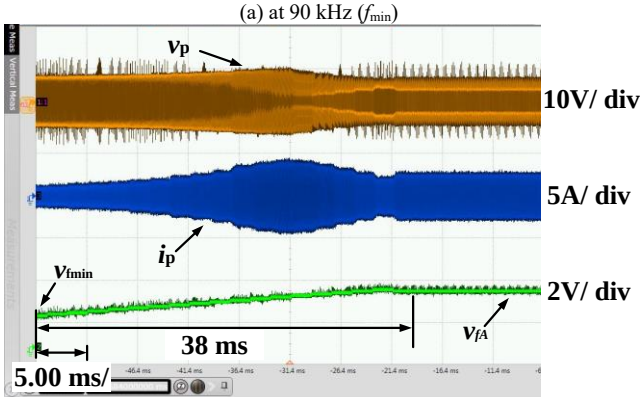

(b) from 90 kHz (f_{min}) to 93.2 kHz (f_A)

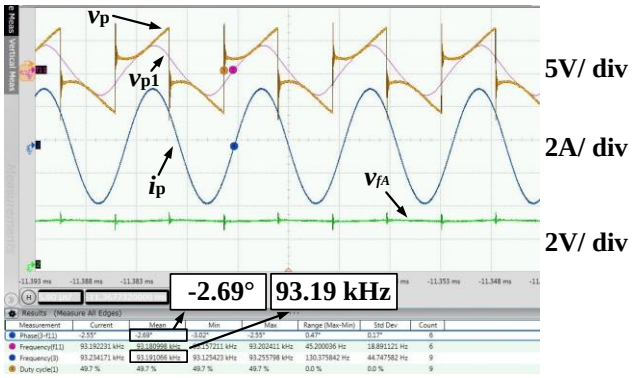

(c) at 93.2 kHz (f_A)

Fig. 25. Waveforms of v_p, v_{p1}, i_p and v_{fp} of the WPT system operating from 90 kHz to 93.2 kHz (10 cm distance between the coils, k=0.17) [23].

Fig. 25 shows the main waveforms of the WPT system when the operating frequency of the WPT system is changed from 90 kHz to 93.4 kHz with the frequency step of 0.2 kHz and then reduced from 93.4 kHz to the critical frequency 93.2 kHz. Based on estimation equation in Fig. 20, the monitored coupling coefficient from the lower bound can be calculated as 0.1728. Similar experiments are also conducted on the WPT system with different distances (or coupling coefficient) between the coils. The comprehensive results are shown in Table II. All the relative errors are less than 5%. The relative errors of the coupling coefficient estimation from either the lower bound or the upper bounds increase when the distance is increased from 10 cm to 18 cm, indicating that the monitoring method is more accurate when the coupling of the coils is stronger. By using the same frequency bounds, the monitoring time from either the lower bound or the upper bound will be increased when the distance is increased. The monitoring times for all the distances are less than 62 ms.

TABLE II. COMPREHENSIVE RESULTS [23]

Distance	Actual k	Monitored k		R_{err}(%)	T_{mon} (ms)
10 cm	0.17	from lower bound	0.1728	1.65	38
		from upper bound	0.1671	1.71	50
12 cm	0.136	from lower bound	0.1384	1.76	52
		from upper bound	0.1329	2.28	22
14 cm	0.111	from lower bound	0.1194	2.05	60
		from upper bound	0.1134	3.08	34
16 cm	0.092	from lower bound	0.0962	2.34	20
		from upper bound	0.09	4.26	48
18 cm	0.076	from lower bound	0.0782	2.89	28
		from upper bound	0.0723	4.87	58

The "hardware-based" method in [23] is also compared to the "model-based" methods in [20-22]. Comparative curves of the relative errors among these methods when the ESR of the transmitter coil deviates about ±2%, ±4% and ±6% while the ESR of the receiver coil remains unchanged. The "hardware-based" method is more accurate than the "model-based" methods in [20, 21] when the ESR of the transmitter coil deviates from the nominal value. Besides, the "hardware-based" method takes much less monitoring time than the "model-based" method in [22].

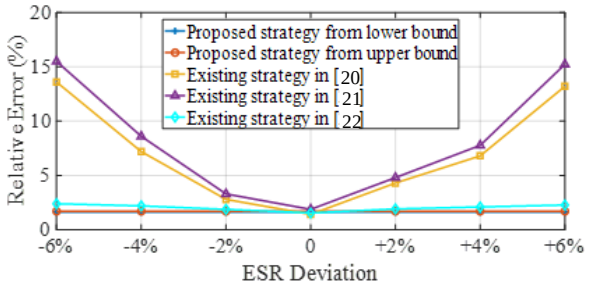

Fig. 26. Comparative curves of the "hardware-based" method and the "model-based" methods [23].

VI. CONCLUSIONS AND FUTURE WORKS

In this paper, the front-end monitoring strategies, including four "model-based" methods and one "hardware-based" method, that have been developed by the Wireless Power Research Group of the University of Hong Kong is presented. Based on the initial work of monitoring a single load in SS-compensated WPT systems, the researchers improve the strategy to monitor the SS-compensated WPT systems with two loads. On the other hand, the monitoring strategy is extended to monitor the load and the mutual inductance simultaneously for a two-stage SS-compensated WPT system. Later on, a simplified load monitoring strategy is further proposed. However, these monitoring methods are designed based on a WPT system with preliminary known parameters. To address the issue of WPT systems with uncertain parameters of the receivers, heuristic algorithm methods are further developed. Nevertheless, these "model-based" methods suffer from either high sensitivity issues of the parasitic parameters or long monitoring time. To this end, a "hardware-based" monitoring strategy is recently proposed to achieve both accurate and fast monitoring at the front-end. However, the "hardware-based" method is only validated for SS-compensated WPT systems with active rectifiers.

In the future works, front-end monitoring based on the dynamic models of the WPT systems maybe a promising strategy, particularly for the moving wireless charging of EV. Besides, front-end monitoring for the WPT systems with LCL-S or LCC-S compensation maybe another research trend, since the advantages of these two compensation schemes over the conventional SS compensation in the applications of EV charging have been

demonstrated. Moreover, the Artificial Intelligence (AI) maybe used to achieve fast online monitoring of mutual coupling and load conditions by considering the parasitic parameters in the resonators and power converters.

REFERENCES

[1] N. Tesla, *On Light and Other High Frequency Phenomena*, Philadelphia: Lecture Delivered before the Franklin Institute, Feb. 1893.

[2] J. C. Schuder, I. H. Gold, and H. E. Stephenson, Jr., "An inductively coupled RF system for the transmission of 1 kW of power through the skin," *IEEE Trans. Biomed. Eng.*, vol. BME-18, no. 4, pp. 265-272, Jul. 1971.

[3] G. A. Covic and J. T. Boys, "Inductive power transfer," *Proceedings of the IEEE*, vol. 101, no.6, pp. 1276-1289, Jun. 2013.

[4] S. Y. R. Hui, "Planar wireless charging technology for portable electronic products and Qi," *Proceedings of the IEEE*, vol. 101, no.6, pp. 1290-1301, Jun. 2013.

[5] M. Treffers, "History, current status and future of the wireless power consortium and the Qi interface specification," *IEEE Circuits & Systems Magzine*, vol. 15, no. 2, pp. 28-31, May 2015.

[6] WPC Qi: https://www.wirelesspowerconsortium.com/qi/.

[7] AirFuel Alliance: https://www.airfuel.com/.

[8] SAE TIR J2954: https://standards.sae.org/wip/j2954/.

[9] C. Jiang, K. T. Chau, C. Liu, and C. H. T. Lee, "An overview of resonant circuits for wireless power transfer," *Energies*, vol. 10, pp. 894, Jun. 2017.

[10] W. Zhang and C. C. Mi, "Compensation topologies of high-power wireless power transfer systems," *IEEE Trans. Veh. Electron.*, vol. 30, no. 11, pp. 6434−6445, Feb. 2015.

[11] N. Y. Kim, K. Y. Kim, J. Choi, and C. W. Kim, "Adaptive frequency with power-level tracking system for efficient magnetic resonance wireless," *Electron. Lett.*, vol. 48, no. 8, pp. 452-454, Apr. 2012

[12] O. C. Onar, J. M. Miller, S. L. Campbell, C. Coomer, C. P. White, and L. E. Seiber, "Oak ridge national laboratory wireless power transfer development for sustainable campus initiative," in *Proc. IEEE Transp. Electrification Conf. Expo.*, Jun. 2013, pp.1-8.

[13] Y. Yang, S. C. Tan, and S. Y. R. Hui, "Communication-free control scheme for Qi-compliant wireless power transfer system," in *Energy Conversion Congress and Exposition (ECCE)*, Sept. 2019, pp. 4955-4960.

[14] A. Namadmalan, "Self-oscillating tuning loops for series resonant inductive power transfer systems," *IEEE Tran. Power Electron.*, vol. 31, no. 10, pp. 7320−7327, Oct. 2016.

[15] Z. Wang, Y. Li, Y. Sun, C. Tang, and X. Lv, "Load detection model of voltage-fed inductive power transfer system," *IEEE Tran. Power Electron.*, vol. 28, no. 11, pp. 5233−5243, Nov. 2013.

[16] Y. G. Su, H. Y. Zhang, Z. H. Wang, et. al., "Steady-state load identification method of inductive power transfer system based on switching capacitors," *IEEE Trans. Power Electron.*, vol. 30, no. 11, pp. 6349–6355, Nov. 2015.

[17] P. Zheng, W. Lei, F. Liu, et. al., "Primary control strategy of magnetic resonant wireless power transfer based on steady-state load identification method," in *IEEE Int. Power Electron. Appl. Conf. Expo.*, Shenzhen, China, Nov. 2018, pp. 1-5.

[18] J. Yin, D. Lin, C. K. Lee, and S. Y. R. Hui, "A systematic approach for load monitoring and power control in wireless power transfer systems without any direct output measurement," *IEEE Tran. Power Electron.*, vol. 30, no. 3, pp. 1657−1667, Mar. 2015.

[19] J. Yin, D. Lin, C. K. Lee, T. Parisini, and S. Y. R. Hui, "Front-end monitoring of multiple loads in wireless power transfer systems without wireless communication systems," *IEEE Tran. Power Electron.*, vol. 31, no. 3, pp. 2510−2517, Mar. 2016.

[20] J. Yin, D. Lin, T. Parisini, and S. Y. R. Hui, "Front-end monitoring of the mutual inductance and load resistance in a series-series compensated wireless power transfer system," *IEEE Trans. Power Electron.*, vol. 31, no. 10, pp. 7339–7352, Oct. 2016.

[21] Y. Yang, Y. Jiang, S. C. Tan, and S. Y. R. Hui, "A frequency-sweep based load monitoring method for weakly-coupled series-series compensated wireless power transfer systems," in *PELS Workshop on Emerging Technologies: Wireless Power Transfer (WoW)*, Montréal, QC, Canada, Jun. 2018, pp. 1-5.

[22] Y. Yang, S. C. Tan, and S. Y. R. Hui, "Front-end parameter monitoring method based on two-layer adaptive differential evolution for SS-compensated wireless power transfer systems," *IEEE Trans. Ind. Informat.*, vol. 15, no. 11, pp. 6101–6113, Nov. 2019.

[23] Y. Yang, S. C. Tan, and S. Y. R. Hui, "Fast hardware approach to determining mutual coupling of series-series-compensated wireless power transfer systems with active rectifiers," *IEEE Trans. Power Electron.*, vol. 35, no. 10, pp. 11026-11038, Oct. 2020.

[24] Y. Yang, W. Zhong, S. Kiratipongvoot, S. C. Tan, and S. Y. R. Hui, "Dynamic improvement of series-series compensated wireless power transfer systems using discrete sliding mode control," *IEEE Tran. on Power Electron.*, vol. 33, no. 7, pp. 6351-6360, Jul. 2018.

[25] H. L. Li, A. P. Hu, G. A. Covic, and C. Tang, "A new primary power regulation method for contactless power transfer," in *Proc. IEEE Int. Conf. Ind. Technol.*, Feb. 2009, pp. 1–5.